

## Hydrothermal alteration and mass exchange in the hornblende latite porphyry, Rico, Colorado

Peter B. Larson<sup>1</sup>, Charles G. Cunningham<sup>2</sup>, and Charles W. Naeser<sup>3</sup>

<sup>1</sup> Department of Geology, Washington State University, Pullman, WA 99164-2812, USA

<sup>2</sup> United States Geological Survey, 959 National Center, Reston, VA 22092, USA

<sup>3</sup> United States Geological Survey, MS 963, Denver Federal Center, Denver, CO 80225, USA

Received March 29, 1992 / Accepted June 30, 1993

**Abstract.** The Rico paleothermal anomaly, southwestern Colorado, records the effects of a large hydrothermal system that was active at 4 Ma. This hydrothermal system produced the deep Silver Creek stockwork Mo deposit, which formed above the anomaly's heat source, and shallower base and precious-metal vein and replacement deposits. A 65 Ma hornblende latite porphyry is present as widespread sills throughout the area and provided a homogeneous material that recorded the effects of the hydrothermal system up to 8 km from the center. Hydrothermal alteration in the latite can be divided into a proximal facies which consists of two assemblages, quartz-illite-calcite and chlorite-epidote, and a distal facies which consists of a distinct propylitic assemblage. Temperatures were gradational vertically and laterally in the anomaly, and decreased away from the central heat source. A convective hydrothermal plume, 3 km wide and at least 2 km high, was present above the stockwork molybdenum deposit and consisted of upwelling, high-temperature fluids that produced the proximal alteration facies. Distal facies alteration was produced by shallower cooler fluids. The most important shallow base and precious-metal vein deposits in the Rico district are at or close to the boundary of the thermal plume. Latite within the plume had a large loss of Na<sub>2</sub>O, large addition of CaO, and variable SiO<sub>2</sub> exchange. Distal propylitized latite samples lost small amounts of Na<sub>2</sub>O and CaO and exchanged minor variable amounts of SiO<sub>2</sub>. The edge of the plume is marked by steep Na<sub>2</sub>O exchange gradients. Na<sub>2</sub>O exchange throughout the paleothermal anomaly was controlled by the reaction of the albite components in primary plagioclase and alkali feldspars. Initial feldspar alteration in the distal facies was dominated by reaction of the plagioclase, and the initial molar ratio of reactants (alkali feldspar albite component to plagioclase albite component) was 0.35. This ratio of the moles of plagioclase to alkali feldspar albite components that reacted evolved to 0.92 as the reaction progressed. Much of the alkali feldspar albite

component in the proximal facies reacted while the primary plagioclase was still unreacted, but the ratio for these assemblages increased to 1.51 when the plagioclase entered the reaction paragenesis. Plagioclase reaction during distal propylitic alteration resulted in pseudomorphic albite mixed with illite and a loss of Na<sub>2</sub>O. CaO is lost in the distal facies as hornblende reacts to chlorite, although some calcium may be fixed in calcite. CaO is added to the proximal facies as the quantity of chlorite replacing hornblende increases and epidote and calcite are produced.

### Introduction

In 1980, Naeser et al. reported that partial annealing of fission tracks in apatite and zircon in 65 Ma hornblende latite porphyry sills (Fig. 1) increases systematically towards the center of the Rico dome, just east of the old mining town of Rico, Colorado. Naeser et al. (1980) and Cunningham et al. (1987) interpreted this pattern to reflect the presence of a young heat source near this center. At about the same time, geochemical exploration and drilling by the Anaconda Company led to the discovery of the deep, large, 4-Ma Silver Creek stockwork molybdenum deposit (Barrett et al. 1985; Larson 1987). Isotopic dating of intrusive rocks and vein minerals (Naeser et al. 1980) indicate that the hydrothermal system related to this heat source produced all of the known ore deposits in the Rico district, and also produced alteration patterns in the latite which extend up to 8 km from the stockwork Mo deposit. These thermal and hydrothermal effects have been designated the Rico paleothermal anomaly (PTA) by Cunningham et al. (1987).

The young age of the hydrothermal system and the ore deposits relative to the host rocks (Precambrian through Cretaceous), the deep drilling, and the presence of a single large hydrothermal system make the Rico PTA ideal for study of the processes of water-rock inter-

action in a continental hydrothermal environment. One km of topographic relief and 1.5 km of diamond drill core provide a vertical interval of more than 2.5 km (more than 8000 ft) from which altered rocks can be sampled. The investigation of the effects of water-rock interaction in the PTA has concentrated on the altered hornblende latite porphyry because: (1) it is widespread throughout the dome and, therefore, records the effects of the PTA from the central heat source to near its known spatial limits, (2) the latite initially had a relatively uniform mineralogy and composition and, thus, the effects of chemical variations in this reactant are normalized, and (3) apatites and zircons from the latite were used by Naeser et al. (1980) to define the PTA. Latite has been collected from throughout the area (Fig. 1), including the localities where Naeser et al. initially collected their fission track samples. The effects of water-rock interaction in forming the ore deposits and the surrounding PTA can, therefore, be interpreted using the time-temperature history of the PTA as measured by the partial to total annealing of the apatite and zircon ages.

Water-rock interaction has produced a variety of mineral assemblages in the latite and has both added and removed major-element components in most samples. The mineral assemblages and their distribution in the alteration facies are described here along with the latite whole-rock major-element compositions and the distribution and compositions of the product and reactant phases. These data are used to define reaction progress and time-integrated mass exchange for some of the major elements that were transported by the hydrothermal fluid. An upright cylindrical volume of altered rock is present directly above the stockwork Mo deposit; we interpret this to mark the location of a hydrothermal

plume above the PTA's heat source (Larson and Zimmerman 1991).

### Geology of the Rico dome

The Rico dome (Fig. 1) is located in southwestern Colorado near the western margin of the San Juan volcanic field (Steven and Lipman 1976). Excellent descriptions and maps of the geology of the dome are by Cross and Spencer (1900), Ransome (1901), Cross and Ransome (1905), Bush and Bromfield (1966), Pratt et al. (1969), McKnight (1974), and Pratt (1976). Recent summaries of the geology and ore deposits of the dome are in McKnight (1974), Naeser et al. (1980), Larson (1987), and Barrett et al. (1985).

The 12 km diameter dome consists of more than 3 km of Paleozoic and Mesozoic sedimentary rocks that have been uplifted more than 1 km. West and northwest trending fault zones intersect in the east-central part of the dome (Fig. 1) and bound a horst of Precambrian greenstone and quartzite at the center of the dome.

There have been two episodes of magmatic activity. The earliest includes two contemporaneous and cogenetic intrusive rocks, hornblende latite porphyry and augite monzonite, which were emplaced about 65 Ma (McKnight 1974; Naeser et al. 1980). The latite occurs as sills and dikes throughout the district, and the monzonite forms a 2.5-km elongate east-west trending stock in the west-central part of the dome (Fig. 1). It appears that no mineralization or alteration were associated with these Laramide-age intrusions. The monzonite is unaltered except along its northern exposure where it is bounded by the east-west fault zone. The younger episode of magmatic activity is characterized chiefly by basaltic, andesitic, rhyolitic, and lamprophyric dikes. One small rhyolitic stock is exposed at Calico Peak (the Calico Peak Porphyry) near the western end of the dome (Larson and Taylor 1987). Isotopic dating of these rocks yields ages between 3.4 and 4.5 Ma, contemporaneous with hydrothermal activity in the district (Naeser et al. 1980).

### Data acquisition

Forty-two samples of the hornblende latite porphyry were collected from throughout the dome (Table 1, Fig. 1). The augite monzonite

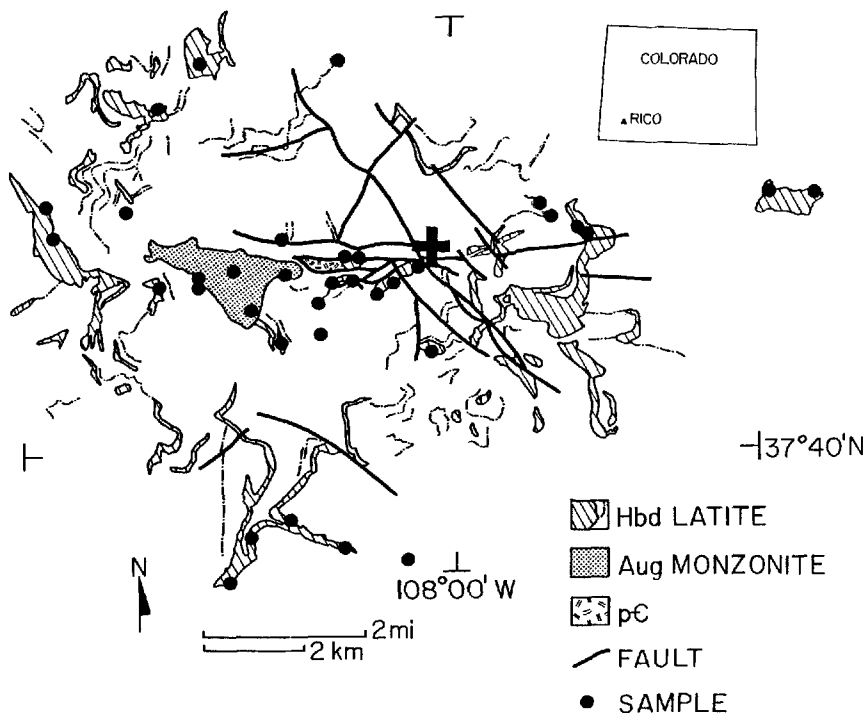


**Fig. 1.** Geologic map of the Rico dome, Colorado, showing the distribution of the hornblende latite porphyry, augite monzonite, the central horst of Precambrian rocks, and major faults (modified from Pratt et al. 1969; McKnight 1974, and Pratt 1976). Sample locations are also shown. The *dark heavy cross* shows the surface projection of the center of the Silver Creek molybdenum deposit. A vertical pole here is the center for the composite radial cross sections (Figs. 3, 4, and 8)

**Table 1.** Locations and alteration facies classifications for the hornblende latite porphyry samples. The locations are relative to the center of the hydrothermal system, the Silver Creek molybdenum deposit (Fig. 1) (108°0.29' N, 37°41.96' W). Azimuths are relative to a vertical pole at the central point and 0° at true North. "Distance to Center" is horizontal distance

Sample number	Distance to center (km)	Azimuth to center (°)	Elevation (m)	Alteration facies <sup>a</sup>
RI-40	3.29	244	2749	PROP
RI-41	7.90	214	2585	PROP
RI-42	6.02	210	2630	PROP*
RI-43	1.65	260	2780	QIC
RI-45	3.01	277	2865	CHL/EPI tr
RI-46	4.31	331	2767	QIC
RI-51	1.51	254	2743	CHL/EPI
RI-52	1.51	254	2743	CHL/EPI
RI-53	2.12	250	2710	CHL/EPI tr
RI-54	7.02	202	2621	PROP
RI-55	1.71	271	2914	QIC
RI-56	1.61	267	2914	QIC
RI-59	Stream float			PROP*
RI-60	5.99	197	2688	PROP
RI-61	5.99	197	2688	PROP
RI-62	5.99	197	2688	PROP
RI-63	5.69	265	3657	PROP \$
RI-64	0.18	257	2963	CHL/EPI
RI-65	0.45	250	2950	QIC
RI-66	0.45	250	2950	CHL/EPI
RI-67	0.45	250	2950	CHL/EPI tr
RI-68	6.04	308	3658	PROP*
RI-70	6.92	293	3597	PROP*
RI-72	7.82	297	3539	PROP
RI-73	7.41	273	3551	PROP*
RI-75	6.27	279	3136	PROP
RI-76	1.84	178	3688	PROP
RI-77	2.37	236	2771	PROP
HP-1	2.29	56	3170	PROP
HP-2	2.27	54	3170	QIC
HP-6	2.94	80	3365	PROP
HP-7	2.98	81	3334	PROP
HP-8	2.39	69	3104	PROP*
HP-9	7.80	80	3529	PROP*
HP-10	7.20	77	3578	PROP*

<sup>a</sup> Alteration facies (see text for descriptions): PROP, propylitic; PROP \$, propylitic with tremolite; PROP\*, propylitic-with-relict-hornblende; CHL/EPI, chlorite and epidote flooding; CHL/EPI tr, transitional between PROP and CHL/EPI; QIC, quartz-illite-calcite

**Table 2.** Concentrations of major elements in representative whole-rock samples of the hornblende latite porphyry and the augite monzonite. Total iron was analyzed as FeO\*

	Latite								Monzonite		
	RI-41	RI-42	RI-43	RI-51	RI-52	RI-53	RI-55	HP-6	HP-8	RI-38	RI-39
SiO <sub>2</sub>	67.65	67.57	67.48	63.05	56.83	67.41	64.58	66.71	62.04	59.69	56.05
Al <sub>2</sub> O <sub>3</sub>	16.20	16.61	16.61	13.27	14.50	17.26	16.69	16.94	16.62	17.74	18.13
TiO <sub>2</sub>	0.424	0.400	0.327	0.700	0.654	0.386	0.399	0.508	0.776	0.876	1.041
FeO*	3.43	3.13	2.53	9.12	8.98	3.06	3.80	4.38	6.27	3.23	7.45
MnO	0.116	0.099	0.178	0.943	0.975	0.221	0.390	0.106	0.158	0.152	0.196
CaO	2.79	2.22	3.92	7.57	11.08	2.26	4.33	0.98	3.65	9.09	8.30
MgO	0.87	0.74	0.71	2.78	2.69	1.01	1.15	1.45	2.12	2.15	2.22
K <sub>2</sub> O	3.27	3.11	2.99	0.27	0.21	3.55	3.74	3.21	2.74	3.78	2.83
Na <sub>2</sub> O	5.94	6.92	4.21	0.14	0.25	4.94	2.90	6.19	5.85	4.63	4.68
P <sub>2</sub> O <sub>5</sub>	0.171	0.181	0.126	0.306	0.293	0.159	0.166	0.225	0.289	0.451	0.567
Total	100.86	100.98	99.08	98.15	96.46	100.26	98.15	100.70	100.51	101.79	101.46

All data are weight percent

**Table 3.** Average electron microprobe analyses and structural formulae for representative feldspar from the hornblende latite porphyry. All formulae are balanced on 8 oxygens. The number of point analyses for each sample is n

n	Alkali feldspar		Plagioclase										
	RI-52 3	RI-63 1	RI-41 4	RI-42 5	RI-43 4	RI-53 10	RI-55 4	RI-59** 2	RI-59 8	HP-6 3	HP-8 7	HP-9** 6	HP-9 3
K <sub>2</sub> O	15.23	15.50	0.20	0.19	0.13	0.13	0.09	0.48	0.04	0.04	0.23	0.41	0.06
Na <sub>2</sub> O	0.47	0.92	10.88	11.49	11.08	11.24	11.45	7.45	11.15	11.45	10.87	7.59	11.37
CaO	0.06	0.04	0.50	0.08	0.37	0.42	0.15	6.66	0.68	0.12	0.75	6.49	0.42
FeO	0.16	0.45	0.01	0.04	0.03	0.01	0.06	0.18	0.02	0.00	0.05	0.26	0.10
BaO	1.10	0.27	0.01	0.02	0.03	0.02	0.03	0.07	0.02	0.04	0.02	0.06	0.01
Al <sub>2</sub> O <sub>3</sub>	19.27	18.40	20.05	19.86	19.73	19.83	19.66	24.86	20.14	19.72	20.24	24.88	19.93
SiO <sub>2</sub>	63.79	64.77	67.13	68.29	67.85	68.02	68.03	60.35	67.76	68.62	67.52	60.30	67.77
Total	100.08	100.36	99.77	99.97	99.22	99.65	99.45	100.05	99.81	100.00	99.67	99.98	99.67
K	0.902	0.912	0.011	0.010	0.007	0.007	0.005	0.027	0.002	0.002	0.013	0.023	0.003
Na	0.042	0.082	0.933	0.973	0.945	0.955	0.975	0.644	0.947	0.968	0.925	0.657	0.967
Ca	0.003	0.002	0.024	0.004	0.017	0.020	0.007	0.318	0.032	0.006	0.035	0.310	0.020
Fe	0.006	0.174	0.000	0.001	0.001	0.000	0.002	0.007	0.001	0.000	0.002	0.010	0.004
Ba	0.020	0.005	0.000	0.000	0.001	0.000	0.001	0.001	0.000	0.001	0.000	0.001	0.000
Al	1.054	1.001	1.045	1.023	1.023	1.024	1.018	1.306	1.039	1.014	1.047	1.308	1.030
Si	2.959	2.989	2.968	2.984	2.985	2.981	2.987	2.690	2.967	2.994	2.962	2.689	2.973
O	8	8	8	8	8	8	8	8	8	8	8	8	8
Or	0.95	0.92	0.01	0.01	0.01	0.01	0.01	0.03	0.00	0.00	0.01	0.02	0.00
Ab	0.04	0.08	0.96	0.99	0.98	0.97	0.99	0.65	0.97	0.99	0.95	0.66	0.98
An	0.00	0.00	0.02	0.00	0.02	0.02	0.01	0.32	0.03	0.01	0.04	0.31	0.02

All analyses are weight percent

\* RI-59\* and HP-9\* are data for unaltered phenocryst cores; all other data are for hydrothermal feldspars

**Table 4.** Average electron microprobe analyses and structural formulae for representative amphibole and sphene from the hornblende latite porphyry. Amphibole formulae were balanced on 22 oxygens and 1 hydroxyl. Sphene was balanced on 4 oxygens and 1 hydroxyl and all aluminum was assumed to be octahedrally coordinated. The number of point analyses for each sample is n

n	Amphibole					Sphene
	RI-42 4	RI-45 3	RI-59 5	HP-8 5	HP-9 5	RI-42 5
CaO	11.22	10.75	11.19	11.60	11.32	27.95
Na <sub>2</sub> O	2.38	2.68	2.08	2.27	2.09	— <sup>a</sup>
K <sub>2</sub> O	1.29	1.60	1.02	0.99	1.16	—
MgO	8.55	8.88	9.73	9.48	9.22	—
MnO	0.72	0.51	0.51	0.53	0.60	0.20
FeO	19.49	18.41	18.17	18.18	18.82	1.42
TiO <sub>2</sub>	1.70	1.72	1.72	2.14	1.75	35.83
Al <sub>2</sub> O <sub>3</sub>	12.04	12.64	12.15	12.18	11.94	1.65
SiO <sub>2</sub>	40.65	40.75	41.76	41.12	41.33	30.11
Total	98.04	97.93	98.33	98.49	98.51	97.22
Ca	1.84	1.76	1.81	1.88	1.84	0.91
Na	0.71	0.79	0.66	0.67	0.79	—
K	0.25	0.31	0.22	0.19	0.31	—
Fe	2.50	2.35	1.92	2.30	2.34	0.04
Mg	1.96	2.02	2.58	2.14	2.01	—
Mn	0.09	0.07	0.07	0.07	0.07	0.01
Ti	0.20	0.20	0.25	0.24	0.20	0.82
Al <sup>(vi)</sup>	0.41	0.50	0.40	0.39	0.46	0.06
Al <sup>(iv)</sup>	1.76	1.78	1.85	1.78	1.80	0.00
Si	6.24	6.22	6.15	6.22	6.20	0.91
O	22	22	22	22	22	4
OH	2	2	2	2	2	1

All analyses are weight percent

<sup>a</sup> for sphene indicates not analyzed

was sampled at five localities. Table 2 lists X-ray fluorescence measurements of major-element concentrations for selected latite and monzonite samples. These data were obtained at Washington State University using standard lithium metaborate fusion techniques. Compositions of minerals in the latite have been measured at Washington State University using standard electron microprobe techniques. Representative data for feldspars, hornblende and sphene, illite, chlorite, calcite, epidote, and magnetite are listed in Tables 3 through 9.

Table 10 shows bulk and powder density measurements for the latite samples. Powder density measurements were made with a pycnometer using splits of powder from the X-ray fluorescence bead preparation. Powder density measurements were conducted for each sample until three successive measurements with a standard deviation less than 0.03 gm/cm<sup>3</sup> were achieved. For most samples this required only 3 or 4 measurements. Bulk densities were determined by measuring the volume of water that a known mass of rock displaced. The rock was first coated with paraffin to seal pore openings. The mass of paraffin was accounted for when the displaced mass of water was measured.

Complete sets of whole-rock and mineral data are available upon request from the first authors.

### The hornblende latite porphyry

All of the samples of hornblende latite porphyry exhibit the effects of interaction with hydrothermal fluids. The alteration of the latite porphyry took place during a single hydrothermal event, and measurable gradational spatial variations of the hydrothermal parameters (e.g., temperature and fluid chemistry) are recorded by spatial variations in the physical and chemical properties of the altered rocks. Here, we describe the primary minerals and the reaction product mineral species in the latite, define alteration assemblages, and discuss the distribution of these assemblages around the thermal center of the PTA.

**Table 5.** Average electron microprobe analyses and structural formulae for representative illite from the hornblende latite porphyry. Illite formulae were balanced on 10 oxygens and 2 hydroxyls. The number of point analyses for each sample is n

	RI-43	RI-46	RI-53	RI-55	RI-56	RI-62	HP-2
n	5	2	5	5	5	3	2
K <sub>2</sub> O	10.42	9.28	10.66	10.77	10.62	10.18	9.41
Na <sub>2</sub> O	0.21	0.12	0.16	0.18	0.15	0.08	0.16
FeO <sup>a</sup>	0.13	0.25	0.53	0.57	0.57	0.28	0.31
Fe <sub>2</sub> O <sub>3</sub> <sup>a</sup>	0.95	1.80	3.77	4.08	4.05	1.97	2.23
MgO	2.28	0.85	1.90	1.78	1.89	1.77	1.24
Al <sub>2</sub> O <sub>3</sub>	31.36	33.20	30.12	29.49	29.30	29.74	31.25
SiO <sub>2</sub>	49.04	50.65	47.06	47.38	47.70	49.70	50.36
Total	94.38	96.13	94.21	94.25	94.28	93.72	94.95
K	0.89	0.77	0.92	0.93	0.92	0.87	0.79
Na	0.03	0.02	0.02	0.02	0.02	0.01	0.02
Fe <sup>2+</sup>	0.01	0.01	0.03	0.03	0.03	0.02	0.02
Fe <sup>3+</sup>	0.05	0.09	0.19	0.21	0.21	0.10	0.11
Mg	0.23	0.08	0.19	0.18	0.19	0.18	0.12
Al <sup>(vi)</sup>	1.74	1.83	1.61	1.59	1.58	1.70	1.75
Al <sup>(iv)</sup>	0.73	0.71	0.80	0.78	0.76	0.66	0.68
Si	3.27	3.29	3.20	3.22	3.24	3.34	3.32
O	10	10	10	10	10	10	10
OH	2	2	2	2	2	2	2

All analyses are weight percent

<sup>a</sup> Total iron was analyzed as FeO and 86.5% was calculated as Fe<sub>2</sub>O<sub>3</sub> (Weaver and Pollard 1973)

**Table 6.** Average electron microprobe analyses and structural formulae for representative chlorite from the hornblende latite porphyry. Chlorite formulae were balanced on 10 oxygens and 8 hydroxyls. The number of point analyses for each sample is n

	RI-41	RI-42	RI-51	RI-52	RI-53	RI-55	HP-6	HP-8
n	4	4	5	5	5	5	5	4
MgO	15.10	14.30	14.11	14.60	16.89	16.15	17.17	16.86
FeO	25.32	25.01	23.01	22.94	21.97	21.39	21.44	22.68
MnO	1.09	1.55	3.31	2.76	1.19	2.73	0.67	1.02
CaO	0.12	0.15	0.03	0.10	0.02	0.05	0.19	0.17
TiO <sub>2</sub>	0.05	0.03	0.05	0.08	0.06	0.06	0.03	0.06
Al <sub>2</sub> O <sub>3</sub>	16.99	18.42	20.81	21.06	20.74	19.82	18.05	17.75
SiO <sub>2</sub>	28.76	28.37	26.32	26.22	26.75	27.55	29.92	29.11
Total	87.44	87.82	87.64	87.76	87.62	87.76	87.46	87.64
Mg	2.38	2.24	2.22	2.29	2.61	2.50	2.63	2.61
Fe	2.24	2.20	2.03	2.02	1.91	1.86	1.84	1.97
Mn	0.10	0.14	0.30	0.25	0.10	0.24	0.06	0.09
Ca	0.01	0.02	0.00	0.01	0.00	0.01	0.02	0.02
Ti	0.00	0.00	0.00	0.01	0.00	0.00	0.00	0.00
Al <sup>(vi)</sup>	1.16	1.27	1.37	1.37	1.32	1.30	1.27	1.20
Al <sup>(iv)</sup>	0.96	1.01	1.24	1.24	1.22	1.13	0.92	0.98
Si	3.04	2.99	2.76	2.76	2.78	2.87	3.08	3.02
O	10	10	10	10	10	10	10	10
OH	8	8	8	8	8	8	8	8

All analyses are weight percent

**Table 7.** Average cation compositions of representative carbonate minerals in the hornblende latite porphyry, calculated from electron microprobe analyses. Total cation charge per formula unit was assumed to be 3. The number of point analyses for each sample is n

	RI-41	RI-42	RI-46	RI-46	RI-51	RI-52	RI-55
n	8	7	4	4	6	8	7
Ca	0.973	0.958	0.901	0.499	0.954	0.966	0.964
Mg	0.004	0.009	0.050	0.362	0.002	0.003	0.007
Mn	0.019	0.021	0.019	0.007	0.037	0.028	0.023
Fe	0.004	0.012	0.027	0.131	0.004	0.002	0.005
Sr	0.000	0.000	0.003	0.000	0.003	0.002	0.001
CO <sub>3</sub>	1	1	1	1	1	1	1

### Primary latite mineralogy: reactants

The primary mineralogy of the hornblende latite porphyry appears to have been nearly uniform throughout the Rico dome, although hydrothermal alteration has now widely destroyed the primary minerals. Every sample of latite that was collected during this study exhibits some effects of hydrothermal alteration. Primary phenocrysts are, in order of abundance, plagioclase, hornblende, magnetite, quartz, sphene, zircon, and apatite. These lie in a fine-grained groundmass of alkali feldspar, plagioclase, and quartz. The phenocrysts make up 35 to 40 vol.% of the rock. Plagioclase is most abundant and usually constitutes about 30 vol.% of the rock. Unaltered plagioclase (sodic andesine, Table 3) phenocrysts are euhedral and tabular, up to 5 mm long, and exhibit oscillatory-normal zoning. Locally, the plagioclase occurs as glomeroporphyritic clots.

**Table 8.** Average electron microprobe analyses and structural formulae for representative epidote from the hornblende latite porphyry. Epidote formulae were balanced on 12 oxygens and 1 hydroxyl. All iron and manganese are assumed to be trivalent. The number of point analyses for each sample is n

	RI-42	RI-51	RI-52	RI-53	RI-55	RI-63
n	5	4	5	5	5	5
CaO	23.02	22.62	23.16	22.95	22.26	23.37
Fe <sub>2</sub> O <sub>3</sub>	12.92	10.58	10.74	13.75	14.62	14.92
Mn <sub>2</sub> O <sub>3</sub>	0.38	1.31	0.95	0.54	1.20	0.08
Al <sub>2</sub> O <sub>3</sub>	23.27	25.55	25.14	22.98	22.16	22.24
SiO <sub>2</sub>	37.83	38.13	38.29	37.94	37.73	37.73
Total	97.42	98.19	98.29	98.15	97.97	98.35
Ca	1.97	1.90	1.95	1.95	1.91	2.00
Fe	0.78	0.63	0.64	0.82	0.88	0.90
Mn	0.02	0.08	0.06	0.03	0.07	0.00
Al	2.19	2.37	2.33	2.15	2.09	2.09
Si	3.02	3.00	3.01	3.02	3.02	3.01
O	12	12	12	12	12	12
OH	1	1	1	1	1	1

All analyses are weight percent

Fresh plagioclase is preserved only as unaltered phenocryst cores in several samples. Hornblende phenocrysts typically account for about 10 vol.% of the rock, and unaltered hornblende (Table 4) is present as euhedral phenocrysts up to 5 mm in length in the least altered rocks.

Quartz, where present, is not more than 2 vol.%, and magnetite, sphene, and apatite are not more than 1 vol.% each. Quartz phenocrysts are not present in all samples, but where present are usually euhedral. Sphene (Table 4) occurs as euhedral phenocrysts up to 3 mm across. Magnetite (Table 9) is widespread, and forms anhedral to euhedral phenocrysts up to 2 mm in diameter. Apatite phenocrysts are sparse but ubiquitous, and have been found in all samples of the latite regardless of the degree of alteration. They

**Table 9.** Average electron microprobe analyses and structural formulae for representative magnetite from the hornblende latite porphyry. Magnetite formulae were balanced on 4 oxygens. FeO\* is the total weight percent of iron measured as FeO. The number of point analyses for each sample is n

	RI-41	RI-42	HP-6	HP-8
n	4	5	2	7
MgO	0.24	0.17	0.11	0.11
Al <sub>2</sub> O <sub>3</sub>	1.03	0.86	0.89	0.79
Cr <sub>2</sub> O <sub>3</sub>	0.04	0.02	0.02	0.09
FeO*	85.83	87.67	82.73	88.53
TiO <sub>2</sub>	3.53	1.88	7.85	2.71
MnO	0.84	0.87	0.01	0.02
SiO <sub>2</sub>	0.27	0.47	0.37	0.23
Total	91.76	91.94	91.96	92.46
Fe <sup>2+</sup>	1.07	1.04	1.24	1.08
Mg	0.01	0.01	0.01	0.01
Mn	0.03	0.03	0.00	0.00
Fe <sup>3+</sup>	1.72	1.81	1.47	1.79
Al	0.05	0.04	0.04	0.04
Cr	0.00	0.00	0.00	0.00
Ti	0.10	0.06	0.23	0.08
Si	0.01	0.02	0.01	0.01
O	4	4	4	4

All analyses are weight percent

typically occur as stubby euhedral crystals up to 1 mm long (rarely to 5 mm). Small needles of apatite occur in both fresh and altered hornblende and in magnetite and quartz. Zircon occurs as fine grains in hornblende and magnetite. Rare, coarse allanite has also been observed.

The groundmass of the latite porphyry consists chiefly of anhedral grains of potassium feldspar molded against one another and mixed with equigranular laths of plagioclase and clots of optically continuous quartz. Small grains of magnetite and other acces-

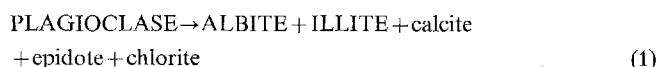
**Table 10.** Densities and porosities of the hornblende latite porphyry samples. The number (n) and standard deviation ( $\sigma$ ) of measurements per sample are tabulated. Porosity ( $\phi$ ) is calculated as:  $\phi = 1 - (\rho_{\text{BULK}}/\rho_{\text{POWDER}})$

	Powder gm/cm**3	n	$\sigma$	Bulk gm/cm**3	n	$\sigma$	Porosity
RI-40	2.667	3	0.004	2.533	6	0.012	0.0502
RI-41	2.667	3	0.011	2.575	6	0.013	0.0345
RI-42	2.609	4	0.011	2.549	6	0.013	0.0230
RI-43	2.650	3	0.007	2.632	4	0.010	0.0068
RI-45	2.623	4	0.020	2.501	8	0.008	0.0465
RI-46	2.675	3	0.009	2.665	5	0.004	0.0037
RI-51	2.887	3	0.019	2.877	5	0.006	0.0035
RI-52	2.971	3	0.020	2.897	5	0.007	0.0249
RI-53	2.603	3	0.024	2.597	6	0.004	0.0023
RI-54	2.599	3	0.015	2.463	5	0.004	0.0523
RI-55	2.701	3	0.012	2.694	5	0.006	0.0026
RI-56	2.713	3	0.010	2.690	5	0.007	0.0085
RI-59	2.656	3	0.021	2.598	4	0.006	0.0218
RI-60	2.606	3	0.020	2.486	6	0.009	0.0460
RI-61	2.637	3	0.025	2.445	6	0.004	0.0728
RI-62	2.646	3	0.011	2.458	6	0.007	0.0711
RI-63	2.680	3	0.014	2.547	5	0.005	0.0496
HP-1	2.649	3	0.011	2.524	5	0.008	0.0472
HP-2	2.681	3	0.007	2.665	5	0.005	0.0060
HP-6	2.628	3	0.012	2.470	5	0.001	0.0601
HP-7	2.659	3	0.013	2.596	5	0.006	0.0237
HP-8	2.772	3	0.011	2.672	5	0.009	0.0361
HP-9	2.642	3	0.009	2.640	5	0.004	0.0008
HP-10	2.660	3	0.010	2.569	5	0.007	0.0342

sory minerals are usually present. Mirolitic cavities lined with euhedral quartz crystals and, very rarely, coarse potassium feldspar crystals are present in several samples.

### Hydrothermal reactions

**Plagioclase products.** Plagioclase is altered to some extent in all of the samples, but even where the alteration products replace the entire primary plagioclase phenocrysts the shapes of the phenocrysts are preserved as perfect pseudomorphs. Two distinct plagioclase reactions have been observed. They can be written in general form as:



where capital letters denote phases that are present in all examples of the reaction, and lowercase letters denote phases that are only locally present in minor quantities. Reaction (1) caused replacement of the plagioclase phenocrysts by relatively-pure albite (anorthite component less than 2 wt %; Table 3, Fig. 2) and illite (Table 5). Calcite (Table 7) is also a common product of this reaction, but it is usually not abundant. Epidote (Table 8) is sometimes present and is less abundant than calcite, and chlorite (Table 6) is rarer than epidote. The calcite, chlorite, and epidote are usually present, together with the illite, as scattered grains enveloped by the secondary albite. Locally, the epidote occurs as large grains within the albite. Typically the albite pseudomorphically replaces the primary plagioclase as a single, optically continuous crystal with the same crystallographic orientation as the original crystal. As a consequence, albite twinning in both reactant and product is parallel to the long dimension of the crystals.

The alteration of the feldspars by reaction (1) is incomplete in several samples, all of which come from areas more than 3 km from the center of the PTA. The partial replacement textures shown by these samples aid in understanding the reaction processes and the variations in the degree of alteration within the PTA. In these samples, albite and illite replace the original plagioclase along grain boundaries, along cracks that penetrate the grains, and along more An-rich zones within the grains. The relict, unaltered patches of plagioclase (sodic andesine) occur as islands within the alteration products, and exhibit typical igneous oscillatory zoning.

Several samples show evidence of the second plagioclase reaction, which completely altered the plagioclase feldspar to coarse, euhedral epidote tablets, calcite, and potassium feldspar. These

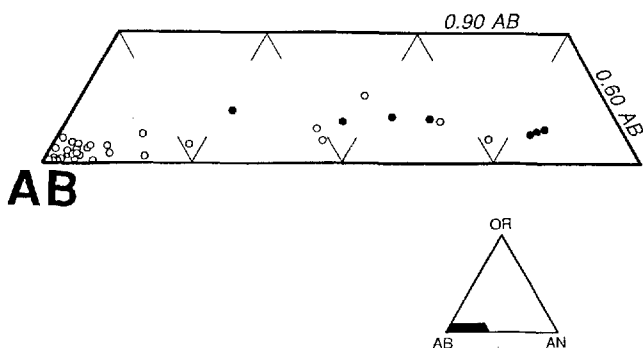
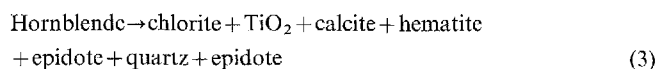


**Fig. 2.** Average plagioclase compositions from the hornblende latite porphyry (Table 3) plotted on the feldspar ternary diagram. The inset (lower right) shows the position of the expanded illustration. Filled circles are unaltered cores of phenocrysts in the least altered samples. Compositions of altered rims for these seven samples all lie in the cluster in the AB corner of the diagram. All other points represent average values for the samples

minerals replace both the plagioclase and marginal line-grained matrix, so it is usually difficult to locate the original plagioclase boundaries.

**Hornblende products.** Hornblende alteration products are diverse, and include chlorite, calcite, illite,  $\text{TiO}_2$ , epidote, quartz, and hematite. The  $\text{TiO}_2$  polymorph has not been positively identified, although spot checks with the electron microprobe have defined the chemical nature of the phase. The proportions of these products vary greatly from sample to sample, and, indeed, within hornblende sites in single samples. Regardless, two distinct hornblende reactions can be recognized:



Reaction (3) is associated with plagioclase reaction (1). Chlorite and  $\text{TiO}_2$  are characteristic alteration products in this reaction, as also are widespread calcite and flakes of specular hematite; epidote, quartz, and illite are sporadic. Reaction (4) caused nearly complete replacement of the hornblende by illite.

The textures in samples which exhibit only partial replacement of the hornblende provide useful information about the reaction process, and these data can be used to define a general reaction paragenesis for the samples that exhibit reaction (3). Initial reaction of the hornblende produces a rim of chlorite and  $\text{TiO}_2$ , with or without hematite, around grain margins and, locally, along penetrating fractures. Alteration proceeds inward from the rims and fractures, and calcite starts to form along with the chlorite as the hornblende is progressively altered. Calcite is found only within the interiors of the altered hornblende phenocrysts, even in samples where the hornblende has been completely altered. Illite may be present in the alteration assemblage, where it probably is later than the calcite, but in most cases the textural relations are obscure. In one sample (RI-61), the illite does seem to be clearly later than the calcite. In this sample, illite penetrates the calcite along fractures, and scattered calcite grains within this illite show optical continuity. Epidote is too sporadic to permit unambiguously assigning it a position in the paragenesis of this reaction scheme, but it appears to be contemporaneous with the calcite.

Thus, for both the primary plagioclase and the hornblende, alteration begins along surfaces where the mineral was in contact with the hydrothermal fluid: phenocryst boundaries and penetrating fractures. Reaction proceeded inward from these surfaces. In reaction (3), the mineralogy of the products evolves as the primary mineral reacts: initially chlorite, hematite, and  $\text{TiO}_2$  are produced, and these are followed successively by calcite and illite. The plagioclase reactions and reaction (4) show no sequential paragenesis.

**Other reactions.** Both sphene and magnetite have been altered in some of the samples. Sphene is either completely altered with formation of  $\text{TiO}_2$ , or completely unaltered. Calcite almost always accompanies the  $\text{TiO}_2$ , and illite, quartz, and epidote have been observed. Altered sphene is characteristic of rocks with intensely altered hornblende. Five of the six samples containing some unreacted hornblende contain fresh sphene (HP-8 is the exception), whereas unaltered sphene was found in only two samples showing complete alteration of the hornblende. Magnetite is partially to totally altered to pyrite in several samples in which pyrite occurs as disseminated grains, reminiscent of the primary magnetite.

Alteration relationships in the groundmass are difficult to observe because of the very small grain size. Under the microscope, alkali feldspar appears clouded with unidentifiable products in most samples. Plagioclase needles have reacted to products similar to those in the phenocrysts.

Apatite was nearly nonreactive during the hydrothermal event, and persists as distinct phenocrysts in all samples. Small, needle-like crystals of apatite, which occur as inclusions in primary hornblende phenocrysts, remain after complete alteration of the hornblende in the most intensely altered latite porphyry.

## Alteration assemblages

On the basis of alteration minerals and textures, we recognize the following alteration assemblages: propylitic, propylitic-with-relict-hornblende, quartz-illite-calcite (QIC), and chlorite-epidote (CHL/EPI). The CHL/EPI assemblage is a propylitic assemblage that exhibits textural features that distinguish it from the propylitic and propylitic-with-relict-hornblende assemblages. These assemblages show a zonal distribution with relation to the heat source for the PTA (Fig. 3). Sample RI-63 exhibits a unique assemblage comprising tremolite, epidote, albite, and illite. Tremolite is not found in any other sample. This assemblage may be important in some areas of the dome, but it is included in the propylitic assemblage until we have more information about its distribution and relationship to the other assemblages.

**Propylitic.** All samples of the latite that are not altered to the QIC or CHL/EPI assemblages in the center of the system, to the limit of the latite's exposure 8 km from the center, exhibit propylitic alteration textures (Meyer and Hemley 1967) that change systematically with distance from the center. This suggests a hydrothermal environment, in which similar rocks reacted, through common processes, with a chemically nearly uniform fluid that existed within a large volume of rock outside the core of the PTA.

Three reactions between primary minerals and the hydrothermal fluid define this assemblage: (a) plagioclase reaction (1), the pseudomorphic replacement of primary sodic andesine phenocrysts to illite and nearly-pure albite, with or without minor calcite, epidote, and chlorite, (b) hornblende reaction (3), alteration of hornblende to form chlorite,  $\text{TiO}_2$ , and usually calcite and hematite, with or without illite and epidote, and with slight overgrowth at crystal margins, and (c) alteration of sphene to form  $\text{TiO}_2$  and calcite, with calcite replacing groundmass minerals adjacent to the sphene.

**Propylitic-with-relict-hornblende.** This alteration assemblage is a subgroup of the propylitic assemblage that occurs within the area of the propylitic assemblage (Fig. 3). It is characterized by relict hornblende as patches within the boundaries of the original crystals. The hornblende and plagioclase reactions are identical to those of the propylitic assemblage. Sphene is usually fresh.

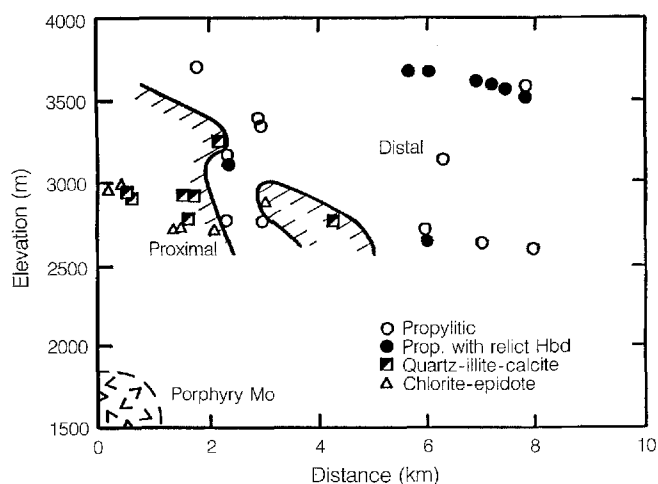


**Fig. 3.** The distribution of hornblende latite porphyry alteration facies plotted on a composite radial cross section. Sample positions are measured relative to a vertical pole through the center of the Silver Creek molybdenum deposit (Fig. 1, Table 1), the thermal center of the Rico hydrothermal system (this construction is also used for Figs. 4 and 8). See text for descriptions of the alteration assemblages, which have been grouped into distal and proximal facies based on their position relative to the porphyry deposit

**Chlorite-epidote (CHL/EPI).** The chlorite-epidote alteration assemblage is present in the latite in the central part of the PTA. No primary minerals are present. Hornblende reaction (3) produced mostly chlorite, with lesser  $\text{TiO}_2$ , epidote, and quartz. Plagioclase exhibits the effects of reaction (2). The alteration products for both reactions pervade the groundmass adjacent to the original crystals. The groundmass consists of coarsely-recrystallized quartz and epidote. Magnetite is either pyritized or absent and former sphene crystals are now irregular clots of  $\text{TiO}_2$ . Epidote veinlets with minor quartz are common.

Latite at several localities near the center of the PTA contains an alteration assemblage that is transitional between propylitic and CHL/EPI. The assemblage is most similar to propylitic, but contains large crystals of epidote replacing up to 50 vol.% of the plagioclase phenocrysts. In contrast, epidote in propylitized plagioclase is usually fine-grained and volumetrically minor. The transitional alteration assemblage is included in the CHL/EPI assemblage in the following discussions.

**Quartz-illite-calcite (QIC).** The QIC assemblage is present both in the central part of the system with the CHL/EPI assemblage and, less commonly, in peripheral propylitized latite (Fig. 3). In both cases, the QIC assemblage is localized along fractures, and its distribution was strongly controlled by permeability. Plagioclase is altered by reaction (1) to albite, calcite, and illite; the illite is coarser than in the propylitized plagioclase. Hornblende reaction (4) resulted in minor chlorite in hornblende sites, but only in the peripheral QIC assemblage. Magnetite is generally pyritized and sphene is altered to  $\text{TiO}_2$  minerals and calcite. The groundmass is a coarsely-recrystallized aggregate of quartz, illite, and calcite.

## Mineral product compositions

The chemical compositions and structures of chlorite, epidote, calcite, and illite vary as a function of alteration assemblage and location within the PTA.

**Illite.** Electron microprobe analyses (Table 5) of the white phyllosilicate occurring as an alteration product of the plagioclase and hornblende and pervasive within the groundmass in the QIC assemblage suggest that it is illite. The structural formulae for the illite, calculated according to Hower and Mowatt (1966), show it to be of intermediate composition in the ternary solid solution series having muscovite, celadonite, and pyrophyllite as pure end members. Total iron was measured as  $\text{FeO}$  and 86.5% of  $\text{Fe}_{\text{total}}$  was assumed to be  $\text{Fe}^{3+}$  in the structural formulae (Weaver and Pollard 1973).

Illites near the center of the PTA generally have a greater muscovite component than illites away from the center, regardless of alteration assemblage. This relationship is consistent with a temperature gradient from high nearest the heat source to cool away from the source. Such variations in illite composition have been observed in active geothermal systems such as the Salton Sea geothermal field, California (McDowell and Elders 1980, 1983), the Coso Hot Springs geothermal system, California (Bishop and Bird 1987), and the Loz Azufres system, Mexico (Cathelineau and Izquierdo 1988). In each of these systems the muscovite component of the illite exhibits a positive correlation with measured temperatures. Cathelineau (1988) used empirical correlations between measured geothermal temperatures and illite compositions to show that the K content and total interlayer occupancy of geothermal illites increase with temperature. Similar variations exist in the Rico illites.

**Chlorite.** Chlorite (Table 6) is an ubiquitous alteration product in the PTA. Its structure and composition vary systematically as a function of its position in the PTA relative to the heat source. Two parameters that vary systematically are: tetrahedral aluminum ( $\text{Al}^{\text{IV}}$ ) and the concentration of manganese. The ratio of iron to magnesium does not exhibit any systematic spatial variation.

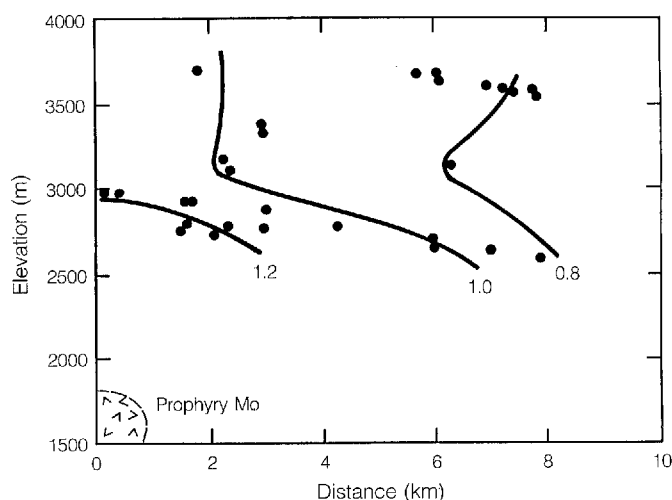


**Fig. 4.** Tetrahedral aluminum in hydrothermal chlorite from the hornblende latite porphyry (Table 6) contoured on the composite radial cross section (see Fig. 3). Average values for each sample are plotted. Tetrahedral aluminum varies as a function of the temperature of formation of the chlorite. The systematic variations show that a thermal gradient was associated with the PTA, with hotter temperatures closer to the porphyry heat source

Cathelineau (1988) has shown that  $Al^{iv}$  substitution in chlorites from active geothermal fields (Salton Sea, Coso Hot Springs, and Los Azufres) varies linearly as a function of measured temperatures, and that lower  $Al^{iv}$  occupancy corresponds to lower temperatures. This linear correlation can be used as a reliable geothermometer in active systems. This application was tested for the fossil geothermal system of the Rico PTA. Figure 4 shows the  $Al^{iv}$  substitution in chlorites of the latite porphyry. The data are shown on a vertical section with the left-hand abscissa being a vertical pole directly over the Mo orebody and the ordinate being distance from the pole in any direction. The  $Al^{iv}$  substitution values define domal contours over the PTA heat source.  $Al^{iv}$  is low (less than 0.8) for samples farthest from the heat source, and high (greater than 1.2) for samples closest to the heat source. These variations are consistent with a thermal gradient with lower temperatures further from the system's center.

Although the chlorite  $Al^{iv}$  substitution varies in a predictable manner, these data yield temperatures, using Cathelineau's (1988) conversion, that appear to be systematically too high. For example, the temperature calculated for the chlorite in RI-41 ( $Al^{iv}=0.96$ ,  $T=247^{\circ}C$ ) would appear to be high for a sample collected 7.9 km from the center of the system. Additionally, a temperature this high, for any geologically reasonable amount of time, would have annealed all of the fission tracks in apatite at this location, yet these apatites show only partial fission track annealing (Nacser et al. 1980). Chlorite temperatures calculated for the central part of the system (greater than  $300^{\circ}C$ ) are significantly higher than fluid inclusion homogenization temperatures for veins (approximately  $200$  to  $300^{\circ}C$ ) from corresponding positions (Larson 1987) and the difference cannot be reasonably ascribed to pressure corrections. The chlorite  $Al^{iv}$  appears to vary in a systematic manner with respect to temperature, but Cathelineau's correlation between these variables does not apply directly to this system and yields temperatures that are too high, perhaps by more than  $50^{\circ}C$ .

The ratio  $Fe:(Fe+Mg)$  in the chlorites does not vary systematically within the Rico system. Values range from 0.37 to 0.63, but most of the ratios lie within the interval 0.4 to 0.5. Values for the proximal CHL/EPI assemblage are 0.42 to 0.48 which is within the broader range of 0.37 to 0.52 exhibited by the propylitic and propylitic-with-relict-hornblende assemblages. Two QIC chlorites have ratios greater than 0.56, but elsewhere in this assemblage chlorites have ratios lower than 0.5. The variation of the chlorite

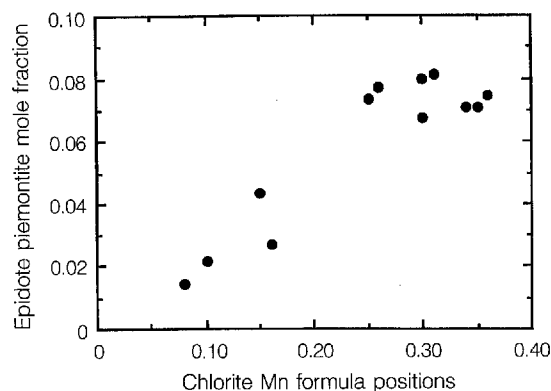


**Fig. 5.** The mole fraction of the epidote piemontite component (Table 8) plotted versus the formula positions of Mn in coexisting chlorite (Table 6) for the hornblende latite porphyry samples. These data define a linear array: Epidote Pm =  $(0.227 \times \text{Chlorite Mn formula positions}) + 0.00688$ , with  $r^2=0.830$

$Fe:(Fe+Mg)$  ratio is best interpreted to suggest that the activities of  $Fe^{2+}$  and  $Mg^{2+}$  in the PTA hydrothermal fluid were variable, but not systematic with respect to location. Note that the  $Fe:(Fe+Mg)$  ratios for primary hornblendes (Table 4) appear to have been nearly uniform and thus did not control the ratio in the secondary chlorite that replaces it.

Mn formula positions in the chlorite increase towards the center of the system. Distal chlorites have less than 0.1 Mn formula positions, and proximal chlorites have 0.3 or greater Mn formula positions. This relationship suggests that the hydrothermal fluid had a higher  $Mn^{2+}$  activity in the central part of the system. Note that Mn minerals (rhodochrosite, rhodonite, and alabandite, McKnight 1974) are locally common in ore deposits in the central part of the Rico dome.

**Epidote.** Epidote in the altered latite (Table 8) is part of the epidote-clinozoisite-piemontite (Ep-Cz-Pm) solid solution series. The CHL/EPI assemblage yields the highest Cz components (0.32 to 0.34) in any of the samples. All of the other samples contain epidotes with Cz components in the range 0.08 to 0.19. Like chlorite, epidote samples near the center of the system contain higher Mn concentrations than samples from distal parts of the system. The formula positions of Mn in chlorites correlate with the Pm component in coexisting epidotes (Fig. 5), indicating both minerals were probably produced in equilibrium with the same fluid.

The distribution of epidote is an irregular dome-shaped configuration at the central part of the system. Although a few locations near the center contain no epidote, it is present only rarely in the periphery. Bird et al. (1984) have noted that epidote occurs in active geothermal systems only where temperatures exceed about  $200^{\circ}C$ . Thus, the limit of the epidote at Rico appears to represent a paleoisothermal surface.

**Calcite.** Carbonate mineral compositions (Table 7) are generally similar. All carbonates have calcite components greater than 0.945, and magnesite, rhodochrosite, and siderite components less than 0.04, except RI-46. The concentration of the rhodochrosite component does not vary with the concentrations of Cz or pennantite components in coexisting epidote and chlorite.

### Major-element exchange in the latite

The hydrothermal system changed the concentrations of most major elements in the latite. Here, the changes in  $SiO_2$ ,  $Na_2O$ , and  $CaO$  are measured relative to  $TiO_2$  and  $P_2O_5$ , whose immobility are demonstrated so that

they can be used as a basis for calculating changes in the other components. The concentrations of  $\text{TiO}_2$  and  $\text{P}_2\text{O}_5$  in the latite appear to have been nearly unaffected by the hydrothermal system. Textural evidence supports this conclusion. Apatite persists as phenocrysts and small needles in virtually all of the samples regardless of alteration assemblage or intensity. The petrographic argument for  $\text{TiO}_2$  is less clear.  $\text{TiO}_2$  minerals are abundant in all sphene and hornblende sites where these minerals are altered, suggesting that although the primary mineral was altered, the  $\text{TiO}_2$  did not migrate far from its original position.

The most significant evidence for immobility of these two components is shown in Fig. 6, a plot of  $\text{TiO}_2$  versus  $\text{P}_2\text{O}_5$  concentrations for all samples of the latite and the augite monzonite, two cogenetic igneous rocks. All five of the monzonite samples are mineralogically and isotopically fresh and thus, the  $\text{TiO}_2$  and  $\text{P}_2\text{O}_5$  concentrations have not been affected by alteration processes. The data on Fig. 6 for both rock types define a smooth linear trend, suggesting that the quantities of  $\text{TiO}_2$  and  $\text{P}_2\text{O}_5$  in the latite have also not changed during hydrothermal alteration. Converting these data to units of mass per unit volume using measured densities for the samples does not change the relationships shown in Fig. 6.  $\text{TiO}_2$  has been chosen as the reference immobile element, although  $\text{P}_2\text{O}_5$  could have been used instead as indicated by their linear relationship in Fig. 6.

The combination of linear trend in Fig. 6 and concordant age determinations (Naeser et al. 1980) suggest that the latite and monzonite are cogenetic, and most of the major element concentrations probably varied linearly between these two units prior to the hydrothermal event. We use this assumption of linearity as a constraint on the initial major element concentrations in the latite. Figure 7 plots the concentration of  $\text{SiO}_2$  in the latite and monzonite as a function of  $\text{TiO}_2$  concentration. The alteration assemblages of the latite samples are coded on Fig. 7. Note that the monzonite and propylitic-with-

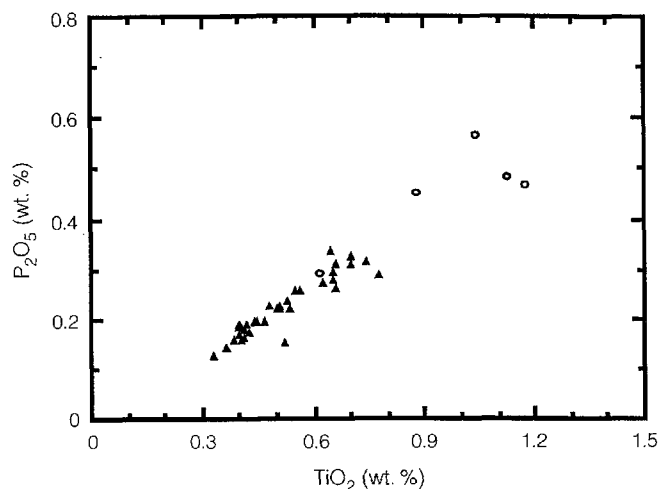


**Fig. 6.** Whole rock  $\text{P}_2\text{O}_5$  plotted against whole rock  $\text{TiO}_2$  for all the hornblende latite porphyry (filled triangles) and augite monzonite (open circles). Data are wt.%. These data support the comagmatic character of these two contemporaneous intrusive units

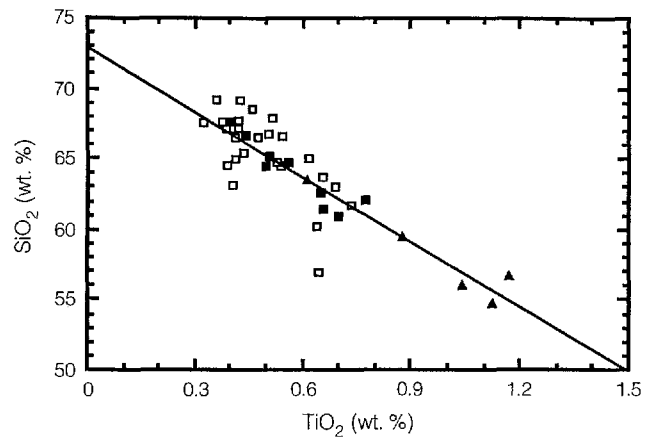


**Fig. 7.** Whole rock  $\text{SiO}_2$  plotted against whole rock  $\text{TiO}_2$  for all the hornblende latite porphyry (squares) and augite monzonite (filled triangles). Data are wt.%. Filled squares, latite samples in the propylitic-with-relict-hornblende assemblage; open squares, all other latite samples. The line is a linear least squares fit to the monzonite and propylitic-with-relict-hornblende latite samples:  $\text{SiO}_2 = (-15.28 \times \text{TiO}_2) + 72.82$ ;  $r^2 = 0.945$

**Table 11.** Mass exchange per REV for  $\text{SiO}_2$ ,  $\text{CaO}$ , and  $\text{Na}_2\text{O}$  in the latite samples. These are calculated using Eq. 1. Equations for the best fit lines used to calculate flux are also tabulated. See text for discussion

	Mass exchange <sup>a</sup>		
	$\text{SiO}_2$	$\text{CaO}$	$\text{Na}_2\text{O}$
m <sup>b</sup>	-15.28	7.977	-3.152
b <sup>b</sup>	72.82	1.160	7.881
r <sup>2c</sup>	0.945	0.720	0.798
RI-40	0.48	0.424	-0.136
RI-41	0.28	-0.035	-0.131
RI-42	0.19	0.079	0.065
RI-43	-0.08	-0.405	-0.587
RI-45	0.18	0.228	0.183
RI-46	-0.63	-0.658	-0.005
RI-51	0.23	-1.035	-1.345
RI-52	-1.51	-2.040	-1.363
RI-53	0.11	0.058	-0.378
RI-54	0.00	0.170	0.056
RI-55	-0.50	-0.448	-0.847
RI-56	-0.86	-0.557	-1.137
RI-59	0.13	-0.001	-0.048
RI-60	-0.36	-0.257	-3.000
RI-61	0.08	0.093	-0.080
RI-62	0.16	0.154	-0.083
RI-63	-0.15	0.016	-0.101
HP-1	0.35	0.610	0.146
HP-2	-0.18	-0.537	-0.886
HP-6	0.35	0.459	-0.019
HP-7	0.22	0.239	-0.159
HP-8	0.25	0.090	0.094
HP-9	-0.26	0.050	-0.120
HP-10	-0.30	-0.080	-0.090

<sup>a</sup> All data are mol/REV (REV = 523.5988 cm<sup>3</sup>)

<sup>b</sup> m and b are the slope and intercept of a line fit to the oxide (y) vs  $\text{TiO}_2$  (x) plot for the monzonite and propylitic-with-relict-hornblende samples

<sup>c</sup> r<sup>2</sup> is the correlation coefficient for this fit

relict-hornblende latite samples define a linear trend. This linear relationship is believed to represent the initial, pre-alteration variation of SiO<sub>2</sub> with respect to TiO<sub>2</sub> in both the latite and monzonite. Petrographic data show that the propylitic-with-relict-hornblende latite has been altered and certainly some components have been added or lost, if only on a minor scale; however, these effects are minimal compared to the rest of the latite. Thus, SiO<sub>2</sub> variations in the other latite samples relative to the line in Fig. 7 are probably the result of the exchange of silica between the fluid and the rock during water-rock interaction.

SiO<sub>2</sub> concentration changed in a systematic manner as a function of alteration assemblage in the latite. Silica has been added to the most intensely propylitized samples, where hornblende has been completely replaced, relative to the propylitized-with-relict-hornblende samples. SiO<sub>2</sub> has been removed from nearly all of the QIC assemblage. The CHL/EPI assemblage generally exhibits an increase of SiO<sub>2</sub>, but one anomalous sample (RI-52) has the lowest SiO<sub>2</sub> concentration of any sample yet measured (56.83 wt.%, Table 2).

Plots similar to Fig. 7 can be constructed for all of the major oxides and can be used to calculate the mass of an oxide component gained or lost ( $M_{ox}$ ) for each sample. For comparison to mineralogical changes,  $M_{ox}$  is calculated on a molar basis for a specific Representative Equivalent Volume (REV, Norton 1984) of rock. The REV is chosen to be a sphere with a radius of 10 cm (523.6 cm<sup>3</sup>). This corresponds approximately to the size of hand specimens collected in the field, and

is several orders of magnitude larger than typical phenocrysts in the latite. Therefore, this volume should be large enough to homogenize small-scale variations in composition and mineralogy, and yet be small enough to be accurately represented by the field samples. The  $M_{ox}$  is determined by calculating the difference ( $\epsilon_{ox}$ ), in weight percent, between the measured oxide concentration and that predicted using a least squares linear fit to the data for the monzonite and least altered latite samples. This difference is converted to  $M_{ox}$  (moles/REV) by

$$M_{ox} = (\epsilon_{ox} * \rho_{BULK} * V_{REV}) / (100 * GFW) \quad (5)$$

where  $\rho_{BULK}$  is the bulk density (gms/cm<sup>3</sup>) from Table 10,  $V_{REV}$  is the volume of the REV (cm<sup>3</sup>), and GFW is the gram formula weight of the oxide. Table 11 compiles  $M_{ox}$  for SiO<sub>2</sub>, Na<sub>2</sub>O, and CaO, and lists the equations that were used to calculate  $\epsilon_{ox}$  for each of them.

### Mineral mass abundances

Mass abundances of the minerals now present in the latite samples have been determined (Table 12). The mass abundances were measured using a combination of point-counting and mass balance calculations of major oxides between mineral and whole rock compositions. A mass balance equation for each oxide can be written (Villas and Norton 1977):

$$C_{11}m_1 + C_{12}m_2 + \dots + C_{1n}m_n = X_1, \quad (6)$$

**Table 12.** Mass abundance<sup>a</sup> of mineral phases in hornblende latite samples

	Qtz	Plag	Ksp	Hbd	Chl	Epi	Mag	Ill	Sphn	Lcx	Apt	Calc	Py
RI-40	1.3972	0.6771	0.7258		0.0582	0.0028 <sup>b</sup>	0.0798	0.0035		0.0307	0.0056	0.0188 <sup>b</sup>	
RI-41	1.4265	0.6752	0.5901		0.0412		0.0482	0.0813		0.0212	0.0037	0.2872 <sup>b</sup>	
RI-42	1.0887	0.8009	0.6281	0.0125	0.0342	0.0050 <sup>b</sup>	0.0408	0.0516	0.0216		0.0040	0.0706 <sup>b</sup>	
RI-43	2.3840	0.7400						0.3867		0.0212	0.0031	0.2035 <sup>b</sup>	0.0868 <sup>b</sup>
RI-45	0.5876	0.7850	0.6675	0.0121	0.0623	0.0596	0.0409	0.0080	0.0421		0.0056		
RI-46	1.0342	0.7458	0.2527		0.1164			0.0329		0.0319	0.0072	0.8689 <sup>b</sup>	0.1471 <sup>b</sup>
RI-51	3.7341		0.0340		0.1616	0.3760				0.0443	0.0068	0.0319 <sup>b</sup>	
RI-52	3.1161		0.0269		0.1560	0.4601				0.0422	0.0063	0.0643 <sup>b</sup>	
RI-53	1.4607	0.8296	0.3662		0.0469	0.1442		0.0310		0.0248	0.0044		0.0118 <sup>b</sup>
RI-54	1.1112	0.8502	0.6117		0.0305		0.0631	0.0712		0.0242	0.0041	0.0298 <sup>b</sup>	
RI-55	2.5064	0.4934			0.0279	0.0490		0.4656		0.0264	0.0037	0.1313 <sup>b</sup>	0.0406 <sup>b</sup>
RI-56	2.8057	0.2821			0.0097	0.0305 <sup>b</sup>		0.6259		0.0271	0.0035		0.1130 <sup>b</sup>
RI-59	1.2222	0.8848	0.4542	0.0627			0.0465	0.0563	0.0156		0.0041		
RI-60	1.3662	0.4919	0.6883		0.0400		0.0379	0.1613		0.0248	0.0040	0.2202 <sup>b</sup>	0.0253 <sup>b</sup>
RI-61	1.4707	0.8269	0.4101		0.0239		0.0506	0.1660		0.0225	0.0041	0.1104 <sup>b</sup>	
RI-62	1.3938	0.7793	0.5204		0.0453		0.0420	0.1187		0.0240	0.0040	0.0591 <sup>b</sup>	
RI-63	0.2681	0.5163	0.8728	0.0756		0.1222		0.0047	0.0324		0.0048		
HP-1	0.9820	0.8502	0.4459		0.1082		0.0702	0.0810		0.0308	0.0059	0.0026 <sup>b</sup>	
HP-2	2.8714	0.4599			0.0913		0.0093	0.3956		0.0282	0.0041	0.1109 <sup>b</sup>	
HP-6	1.2294	0.7601	0.5207		0.0617		0.0693	0.1320		0.0161	0.0050		
HP-7	1.4203	0.7073	0.5313		0.0759		0.0586	0.0897		0.0268	0.0048	0.0905 <sup>b</sup>	
HP-8	0.9245	0.7336	0.4198	0.0266	0.1009	0.0013 <sup>b</sup>	0.0678	0.0964		0.0267	0.0063	0.1533 <sup>b</sup>	
HP-9	0.9512	0.6475	0.6386	0.0347	0.1026			0.0211		0.0380	0.0070	0.0884 <sup>b</sup>	0.0201 <sup>b</sup>
HP-10	0.9461	0.7634	0.6798	0.0356	0.0633			0.0011		0.0348	0.0068	0.0241 <sup>b</sup>	0.0039 <sup>b</sup>

<sup>a</sup> All data are mol/REV (REV = 523.5988 cm<sup>3</sup>)

<sup>b</sup> Data determined from point counting, all other data calculated using mass balance between whole rock and mineral compositions (see text). Blank spaces indicate mineral absence from a sample.

Mineral abbreviations are: qtz, quartz; plag, plagioclase; ksp, alkali feldspar; hbd, hornblende; chl, chlorite; epi, epidote; mag, magnetite; ill, illite; sphn, sphene; lcx, TiO<sub>2</sub>; apt, apatite; calc, calcite; py, pyrite

**Table 13.** Comparison between point counting and mass balance calculated volumes for chlorite and hornblende in several of the latite samples

	Chlorite		Hornblende	
	Calculated <sup>a</sup>	counted <sup>a</sup>	Calculated <sup>a</sup>	counted <sup>a</sup>
RI-41	4.28	5.25		
RI-42	3.60	4.15	1.73	1.85
RI-52	18.34	17.50		
RI-59	0.00	0.18	8.81	8.18
HP-1	11.20	11.70		
HP-7	7.99	7.30		
HP-9	11.18	10.30	4.97	4.85
HP-10	6.58	8.35	4.87	5.70

<sup>a</sup> vol.%

where  $C_{ab}$  is the concentration of oxide a in phase b,  $m_b$  is the concentration of mineral b in the rock, and  $X_a$  is the concentration of oxide a in the rock, all in weight fractions. These define a series of n simultaneous linear equations for each sample. This series of equations can be solved for the weight fraction of minerals in the rock if the number of oxide components is equal to the number of phases; that is, if the oxide concentrations in the minerals define a square matrix. These equations have been solved algebraically for all of the samples for which complete whole-rock (Table 2) and electron microprobe analyses for the constituent minerals (Tables 3 through 9) have been completed. The solutions were obtained using the Gauss reduction method (see, for example, Hildebrand 1974) by programming a spreadsheet on a desk-top computer.

The volumes of calcite and pyrite in each sample were determined by standard point counting techniques (generally 2000 points per sample). Epidote quantity was also determined using point counting where it was present in small mounts (less than about 1%). The volumes of chlorite and hornblende were also measured in some samples during point counting to check the accuracy of the mass abundance calculations. The comparisons between the results of the point counting and mass abundance calculations (Table 13) appear to be very good.

Nearly every latite sample contains a unique set and number of phases, and Eq. 6 was therefore solved on a sample by sample basis. Determination of the weight fraction of minerals in propylitic, propylitic-with-relict-hornblende, and CHL/EPI samples usually required an 8 by 8, 7 by 7, or 6 by 6 matrix; however, samples with QIC alteration products could usually be solved with a 3 by 3 or 4 by 4 matrix using only selected oxides. For example,  $\text{SiO}_2$ ,  $\text{Al}_2\text{O}_3$ ,  $\text{K}_2\text{O}$ , and  $\text{Na}_2\text{O}$  were used for plagioclase, quartz, illite, and chlorite in RI-56. The oxide concentrations in the whole rock were adjusted prior to the calculations to account for CaO in calcite, Fe (converted to  $\text{FeO}^*$ ) in pyrite, CaO in apatite (assuming all  $\text{P}_2\text{O}_5$  is in pure hydroxyapatite), and  $\text{Fe}_2\text{O}_3$ ,  $\text{Mn}_2\text{O}_3$  (both converted to divalent oxide concentrations), CaO,  $\text{Al}_2\text{O}_3$ , and  $\text{SiO}_2$  in epidote if it was present.

The results obtained from Eq. 6 were combined with the point counting results to produce a complete inven-

tory of the weight fractions of all solid phases in the samples. These data were then converted to moles/REV, accounting for porosity (Table 10) by first converting the weight fractions of the minerals to moles/gram (mineral densities from Helgeson et al. 1978, and Robie et al. 1978), and then normalizing these results to the volume of the REV using the bulk density data from Table 10. The results of these calculations are shown in Table 12.

## Discussion

The two most abundant primary phenocryst phases in the latite, plagioclase and hornblende, exhibit reactions which have been used to define the alteration assemblages. The mass exchange of the major oxides varies systematically with the assemblage, and spatial patterns of net gain or loss of a component are related to the paleohydrology of the system. Comparisons between the mass of alteration minerals and the mass exchange of major components among the samples permits us: (1) to compare mass exchange to the mineralogic changes in the rocks, (2) to determine the masses of primary minerals that have been destroyed as a function of alteration assemblage, and (3) to evaluate the paths of reactions.

### Mass exchange and the thermal plume

Nearly all of the original sodium has been leached from the latite in a cylindrical volume directly above the stockwork molybdenum deposit (Fig. 8). The near-vertical, closely-spaced contours of sodium mass exchange are interpreted to mark the edge of the cylinder, within which the upwelling hydrothermal fluids formed a plume

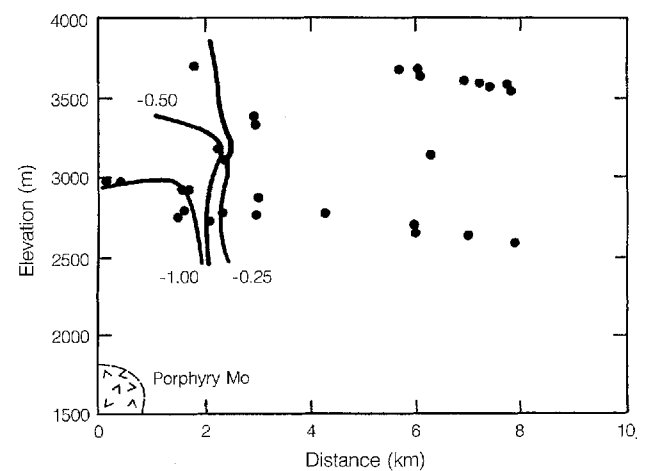


**Fig. 8.** Sodium contents of the latite samples contoured on the composite radial cross section (see Fig. 3). Contoured units of mass exchange are moles of oxide per REV. A vertical cylinder characterized by intense sodium depletion and having steep lateral gradients is above the PTA's porphyry heat source. This zone coincides with the distribution of the proximal alteration facies (Fig. 3) and is interpreted to represent the location of a thermal plume associated with the PTA.

above the Mo deposit and its related intrusion. This interpretation is consistent with theoretical models of convective fluid flow around cooling plutons (Norton 1982; Norton and Knight 1977), which show that less dense heated waters rise above a heat source and penetrate lower temperature denser waters. The plume was about 3 km in diameter and can be traced vertically from the stockwork Mo deposit upwards more than 2 km.

Other data support the plume interpretation. Alteration in the central part of the system occurred at higher temperatures than in the periphery, as indicated by the variation in the concentration of aluminum in the chlorite tetrahedral site (Fig. 4) and by the total annealing of fission tracks in the center of the PTA (Naaser et al. 1980). The outer edge of the volume of sodium loss also coincides with the inner limit of the distribution of the distal propylitic alteration assemblages (Fig. 3). This suggests that two thermally and chemically distinct fluids were present in the PTA: a hot fluid upwelling from a deep source that produced the proximal facies, and a heated but cooler, upwelling shallow fluid in the periphery that produced the distal facies. The location of the plume also coincides with the zone in which many of the major high angle faults in the Rico dome intersect; these would have provided channels for directing hydrothermal fluid flow. It is also important to note that much of the base and precious metal production from veins in the Rico District was from areas on or very close to the outer boundary of the plume (for example, the Newman Hill and CHC Hill areas; McKnight 1974; Larson 1987).

Mass exchange of silicon and calcium is also greatest in the area of the plume. CaO has been added to most of the proximal samples. SiO<sub>2</sub> exhibits antithetic behavior between the two proximal assemblages: it is enriched in the QIC and depleted in the CHL/EPI assemblages. The absolute values of the exchange for these two components (and most of the other major elements) are greatest in the plume area regardless of alteration assemblage.

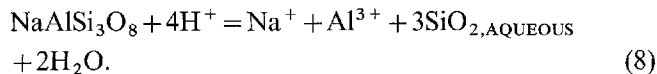
#### *Sodium exchange and changes in the albite component*

Sodium occurs mostly in the albite components in plagioclase and alkali feldspar, both of which are primary minerals in the latite. The mass exchange of Na<sub>2</sub>O can, therefore, be related to changes in the masses and compositions of these two minerals as a function of the alteration progress. The extent of reaction in an open hydrothermal flow system can be measured with the reaction progress variable,  $\xi$  (De Donder and Rysselberghe 1936). The change in moles of a mineral  $i$ ,  $dn_i$ , in a chemical system is related to the reaction progress variable by Brimhall (1979)

$$dn_i = v_{i,\Phi} d\xi \quad (7)$$

where  $v_{i,\Phi}$  is the stoichiometric reaction coefficient for mineral  $i$  and a particular net reaction  $\Phi$ , and  $\xi$  is an overall reaction progress variable (Brimhall 1979). It is most convenient, for reasons given below, to use the

albite component in the plagioclase as the index reactant mineral. Reaction of the albite component can be written



This form of the albite reaction is convenient because the albite component does not exhibit a solid-phase product in the distal facies, where it decreases in mass as a function of other chemical exchange in the samples. Then, following Brimhall (1979), Eq. 7 can be integrated to yield

$$\xi_{\text{AB}} = (0.75 - n_{\text{AB}}) / 0.75 \quad (9)$$

where  $n_{\text{AB}}$  is the number of moles of albite plagioclase component that remain in an altered sample. 0.75 is the estimated typical molar mass of albite reactant in the initial, unaltered latite.  $\xi_{\text{AB}}$  is calculated from Eq. 9 and data from Table 12. Figure 9 shows  $\xi_{\text{AB}}$  plotted against the sodium mass exchange. An  $M_{\text{Na}_2\text{O}}$  of 0.0 on the y axis for  $\xi_{\text{AB}}$  of 0 marks the position of initial plagioclase albite component in the latite (35 to 45 vol.% plagioclase, An<sub>35</sub>), although some of the latite samples must have exhibited some minor variations from its initial position.

If the sodium produced by reaction (8) is removed totally from the rock, then each mole of albite in an REV that reacts will result in the loss of 0.5 moles of Na<sub>2</sub>O from that REV. Thus, reaction of the albite component of plagioclase with total sodium loss would produce a downward trajectory with a slope of  $-0.425$  on

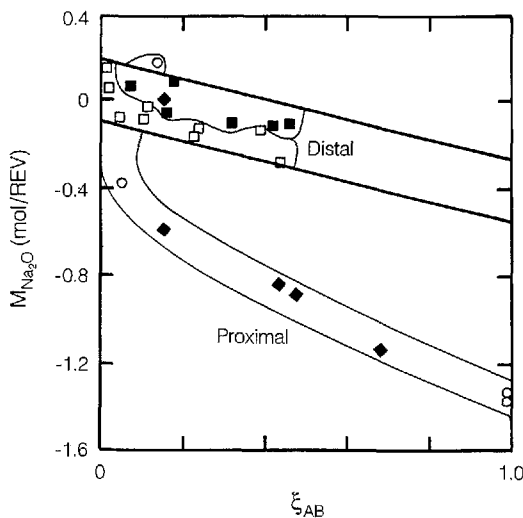


**Fig. 9.**  $\xi_{\text{AB}}$  versus the sodium mass exchange (mol/REV) for the latite samples. Data points are coded as per alteration assemblage: filled squares, propylitic-with-relict-hornblende; open squares, propylitic; open circles, CHL/EPI; filled diamonds, QIC. Two lighter lines with slopes of  $-0.425$  bracket the distal field and are theoretical limits for a process in which the albite component of the plagioclase reacts and the product sodium is removed from the sample, and in which the initial albite component of the alkali feldspar does not react. Samples of the proximal alteration facies define two trajectories, one horizontal and one with a positive slope. Distal facies samples lie in two distinct fields. See text and Fig. 10 for discussion

Fig. 9, away from the initial rock position. Note here that the  $\xi_{AB}$  axis in Fig. 9 records only the reaction of the plagioclase albite component and does not include reaction of the albite component of the primary alkali feldspar. Therefore, reaction of the albite component in the alkali feldspar with no reaction of the component in the plagioclase would produce a vertical downward trajectory in Fig. 9.

The proximal and distal facies define two distinct fields on Fig. 9. The proximal (QIC and CHL/EPI) facies field initially shifts down from the primary rock, and then projects to the right through a well-defined linear array of data with a slope of  $-0.905$  defined by a least squares fit of the data. The distal facies lie in two subparallel fields that are completely bracketed by the theoretical limits of sodium loss due to plagioclase albite component removal. The slope of the propylitic data array is  $-0.692$  (least squares fit).

The field of propylitic-with-relict-hornblende has a slope on Fig. 9 ( $m = -0.486$ , least squares fit), although these samples were used with the monzonite data to define  $M_{Na_2O}$  and these data might be expected to scatter closely about the origin of the abscissa. It is possible that the line used to calculate  $M_{Na_2O}$  does not really fit an assumed initial linear array of data for fresh latite samples. The slope of the propylitic-with-relict-hornblende data (and, indeed, of the data for the other assemblages as well) could, therefore, be a function of the skewness of these two lines. This possibility can be tested because it would produce a systematic relation between  $M_{Na_2O}$  and  $TiO_2$ , that is,  $M_{Na_2O}$  would vary as a function of distance along the  $TiO_2$  axis from the point of intersection of the two lines ( $M_{Na_2O}$  would increase as the separation between the two lines increased). Such a plot reveals no such variation and we can, therefore, proceed with some confidence that the trends shown in Fig. 9 are real.

The distinct proximal and distal trends in Fig. 9 show that feldspar alteration in these two facies proceeded along different trajectories with different, but internally consistent, molar ratios of plagioclase to alkali feldspar reactants. The slopes for the four distinct trajectories in Fig. 9 can be used to calculate the ratio,  $r$ , of the moles of the alkali feldspar albite component ( $A_K$ ) to moles of the plagioclase albite component ( $A_P$ ) that have reacted to produce each trajectory, where

$$r = A_K/A_P. \quad (10)$$

Each trajectory can be represented by a reaction vector (Fig. 10a), where their origins have been normalized to the initial latite. The four reaction vectors are each the sum of two scaled component vectors,  $\mathbf{K}$  and  $\mathbf{P}$ , which are defined on Fig. 10b by the reaction of one hypothetical mole of the albite component in the alkali feldspar and plagioclase, respectively, with complete loss of sodium from the REV. The two scalar quantities are  $A_K$  and  $A_P$  for  $\mathbf{K}$  and  $\mathbf{P}$ , respectively. The magnitude of the scalar quantities for each reaction vector will vary as a function of the length of the reaction vector. However, the ratio of the two scalar quantities,  $r$ , for each of the four reaction vectors will be constant for any

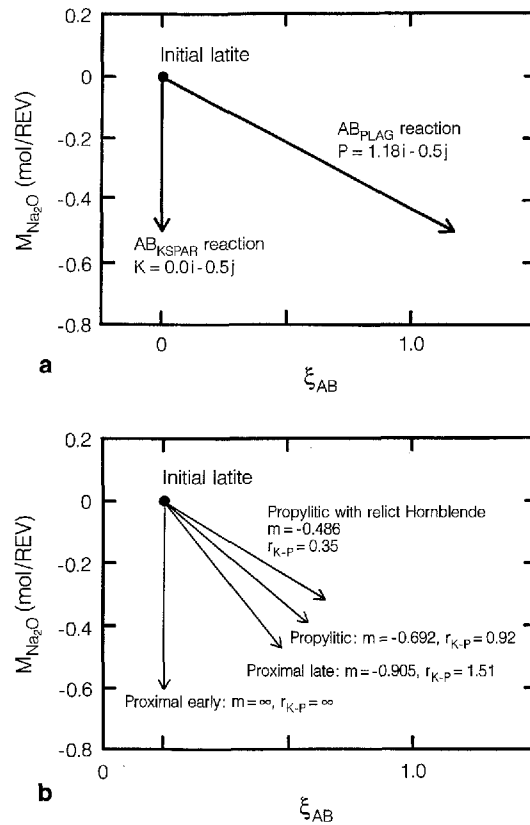


**Fig. 10a, b.** Vector analyses of the reaction paths shown in Fig. 9 plotted on these same axes. **a** The two vectors  $\mathbf{K}$  ( $AB_{KSPAR}$ ) and  $\mathbf{P}$  ( $AB_{PLAG}$ ), drawn to scale, represent independent reaction of one mole of the albite components of alkali feldspar and plagioclase, respectively. The vector  $\mathbf{P}$  has a slope of two and was used to construct the plagioclase reaction brackets in Fig. 9. **b** Four vectors, not scaled, are theoretical fits of  $\mathbf{K}$  and  $\mathbf{P}$  to the four distinct reaction trajectories in Fig. 9. These models correlate with trajectory slopes ( $m$ , linear least squares fits) and the reaction ratios of the moles of plagioclase to alkali feldspar's albite components ( $r$ ) for the four trends. See text for methods of calculation and discussion

point along the length of each reaction vector. The two scaled component vectors can be written

$$A_K \mathbf{K} = A_K(0.0\mathbf{i} - 0.5\mathbf{j}) \quad (11)$$

$$A_P \mathbf{P} = A_P(1.1765\mathbf{i} - 0.5\mathbf{j}). \quad (12)$$

An arbitrary reaction vector,  $\mathbf{L}$ , can be written as the sum of the two scaled component vectors (11) and (12)

$$\mathbf{L} = (1.1765A_P)\mathbf{i} - 0.5(A_P + A_K)\mathbf{j}. \quad (13)$$

The slope of  $\mathbf{L}$ ,  $m$ , is then

$$m = -0.5(A_P + A_K)/1.1765A_P. \quad (14)$$

Combining EQs. 10 and 14 then yields

$$r = m/(2-m). \quad (15)$$

Equation 15 has been applied to the four reaction trajectories in Fig. 9, and the results are shown in Fig. 10a.

The molar ratio,  $r$ , of the albite components in the alkali feldspar and plagioclase that react during propylitic-with-relict-hornblende alteration is 0.35. For propylit-

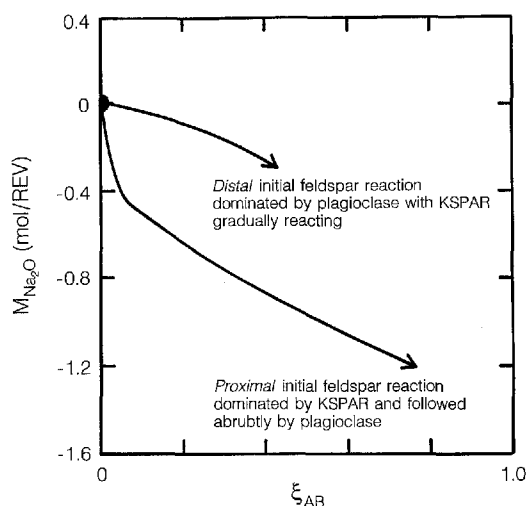


Fig. 11. Schematic reaction trajectories for the distal and proximal trends shown in Figs. 9 and 10. See text for discussion

ic alteration  $r$  is greater, 0.92. The propylitic-with-relict-hornblende alteration appears both texturally and spatially to be an early stage of the propylitic assemblage. Thus, feldspar alteration in the distal facies is dominated during early stages of the reaction by plagioclase, but alkali feldspar dominates the feldspar reactions as the reaction progresses (Fig. 11). The spread and overlap of data for these two facies in Figure 9 suggest that the transition from plagioclase to alkali feldspar domination is gradational.

The feldspar reaction path in the proximal facies is distinct from that in the distal facies (Fig. 11). The proximal feldspars appear to react in a two-stage paragenesis, each with a nearly constant ratio,  $r$ . The first stage is dominated by mobility of the alkali component in alkali feldspar and includes little, if any, in the plagioclase. The second stage involves both feldspars and has a well-defined ratio,  $r$ , of 1.51 ( $r^2$  for this data set is 0.982). This is greater than the ratio for the propylitic assemblage, 0.92 (Fig. 10a). All of the primary alkali feldspar occurs in the groundmass of the latite samples, and in both proximal assemblages, CHL/EPI and QIC, has been coarsely recrystallized and replaced by minerals that do not include a feldspar or a Na-rich phase. In contrast, the groundmass in the distal facies appears nearly fresh in most samples. Figures 9 and 10 suggest, therefore, that much of this groundmass alteration may have occurred prior to eventual alteration of the plagioclase phenocrysts.

#### Chlorite production and hornblende reaction

Chlorite is the most widespread and abundant alteration product from hornblende: it occurs in all assemblages in former hornblende sites and, in the propylitic-with-relict-hornblende assemblage, in intimate reaction relationships with its parent. Unfortunately, chlorite is not the only hornblende product and it occurs in variable proportions with a number of other alteration minerals.

Therefore, it is difficult to use the mass of chlorite in a sample as a comparative monitor of reaction progress without considering the mass of hornblende that has been reacted and the mass of other products of the reaction.

One method is to compare the mass of chlorite to the mass of a component that is produced during alteration of hornblende but that is not concentrated in the chlorite. CaO is such a component. Figure 12 compares the CaO to the mass of chlorite in the REV. Note that each assemblage has a distinct field on Fig. 12. The field for propylitic-with-relict-hornblende shows no CaO exchange related to chlorite production, but this assemblage is defined as "unaltered" for the mass exchange calculation. Although Ca-bearing phases in these samples do show reaction relationships (hornblende is partially altered in nearly all of these samples), the positions of the fields for other assemblages would not shift relative to this field even if a different line was used to calculate the  $M_{CaO}$  values. Note also that primary plagioclase is also a primary Ca reservoir in the rock. However, in most samples the plagioclase has been altered to nearly pure albite (Fig. 2), and this reaction's effect on the calcium mass exchange is somewhat normalized.

With these limitations in mind, Fig. 12 provides useful information about the hornblende reaction and the CaO mass exchange. The field for the propylitic assemblage has a negative slope leading up and away from the propylitic-with-relict-hornblende samples. Figure 12 also shows contours of the mass of calcite (mol/REV) for the propylitic samples. These contours lie nearly normal to the  $M_{CaO}$  axis and exhibit a correlation between lower calcite concentrations and greater CaO loss from the REV. This relationship suggests that some of the calcium liberated by hornblende (and plagioclase) reaction can be fixed in the rock if the activity of  $CO_2$  in the hydrothermal fluid is high enough to stabilize calcite. Figure 12 also suggests that more chlorite will be produced by hornblende reaction if less calcium is fixed

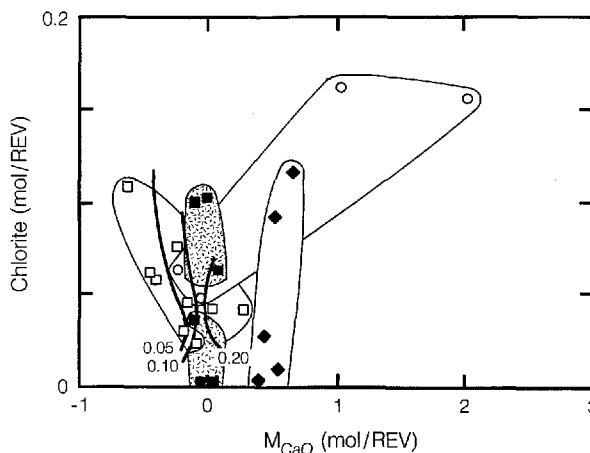


Fig. 12. The mass of chlorite now present in the latite samples versus their calcium mass exchange, both in units of mol/REV (moles oxide for the calcium). Symbols as for Fig. 9. The moles of calcite in an REV are contoured for just the propylitic (open squares) samples. See text for discussion

in calcite. This is an interesting relationship, because these two alteration minerals share no common major oxide components.

The proximal facies contains increased CaO in contrast to the distal facies. The QIC samples in Fig. 12 define a narrow vertical field displaced about 0.5 mol/REV to the right of and parallel to the propylitized-with-relict-hornblende field. The only significant Ca-bearing phase in the QIC samples is calcite, which has a uniform composition among all the QIC samples (Table 7). The linearity of the QIC field shows that a uniform quantity of Ca is added to, and fixed within, the rock during QIC alteration. The CHL/EPI samples have both gained large masses of CaO, with Ca fixed in the epidote, and high concentrations of chlorite.

### Summary and conclusions

Some important conclusions of this study are summarized here.

(1) The hydrothermal system that produced the Rico paleothermal anomaly affected a large volume of rock surrounding the Mo deposit. Thermal and hydrothermal effects of the PTA in the older hornblende latite porphyry are gradational and center both vertically and horizontally on the Silver Creek stockwork molybdenum deposit, which is located 1200 m below the present ground surface in the central part of the district. Intrusive activity associated with the deposit was the heat source for the PTA. Paleotemperatures increase towards the deposit as indicated by increasing tetrahedral Al in chlorite, higher degrees of fission track annealing (Naeser et al. 1980), and fluid inclusion geothermometry (Larson 1987).

(2) Alteration assemblages in the latite are also zonally distributed about the Mo deposit. The proximal facies includes the QIC and CHL/EPI assemblages, which are present in the central part of the system directly over and around the heat source. The distal facies includes a propylitic assemblage which locally contains unreacted hornblende (propylitic-with-relict-hornblende assemblage).

(3) A convective hydrothermal plume existed above the heat source during formation of the PTA. The plume was 3 km wide and more than 2 km high within its present level of exposure. The plume contained hotter upwelling fluid that produced the proximal facies alteration. The part of the fossil hydrothermal convection cell now exposed outside the plume was formed by cooler upwelling fluids that produced the distal alteration facies in the latite. The vertical contact between the two fluids was sharp and is marked by chemical and mineralogical changes.

(4) Feldspar reactions in the distal and proximal facies followed two different reaction paths, both of which included the loss of sodium from the latite. Initial reaction in the proximal facies involved only alkali feldspar, but evolved to include plagioclase. The feldspar reactions in the distal facies began with plagioclase predominating over alkali feldspar (0.35 molar ratio of reacted

alkali feldspar to reacted plagioclase albite components) but progressed to greater alkali feldspar participation (0.92 molar ratio of reacted alkali feldspar to reacted plagioclase components). The plagioclase in the distal facies is pseudomorphically replaced by albite, illite and other, minor, products, but this albitization actually occurs with a net loss of sodium and does not represent sodium metasomatism.

(5) Hornblende reactions in the latite can be evaluated by comparing CaO mass exchange to the development of hydrothermal chlorite. Propylitized samples contain chlorite replacing hornblende with a related loss of calcium, but calcite may be produced at the expense of the chlorite. Samples of the proximal facies typically show CaO enrichment that is related to the production of calcite and epidote.

*Acknowledgements.* We are grateful to Don Cameron, John Wilson, and Larry Barrett, who have shared their knowledge of the Rico area and provided access during the early stages of this study. Wayne Webster also was helpful in providing access. Clive Rice, Tom Steven, Brian Zimmerman, Jeff Brooks, Hugh Taylor, and Chris Wareham contributed useful discussions. Brian Zimmerman and Andy James were instrumental in helping complete the laboratory analyses. Paul Barton, George Erickson, Denis Norton, and an anonymous reviewer provided detailed and most useful reviews from which the manuscript received a great deal of benefit. This work was supported by National Science Foundation grant EAR-8903492.

### References

- Barrett LF, Cameron DC, Wilson JC (1985) Discovery of the Silver Creek molybdenum deposit, Rico, Colorado. *Trans Am Inst Min Metall Petr Eng.* Preprint 85-118
- Bird DK, Schiffman P, Elders WA, Williams AE, McDowell SD (1984) Calc-silicate mineralization in active geothermal systems. *Econ Geol* 79:671-695
- Bishop BP, Bird DK (1987) Variation in sericite compositions from fracture zones within the Coso Hot Springs geothermal system. *Geochim Cosmochim Acta* 54:1245-1256
- Brimhall GH Jr (1979) Lithologic determination of mass transfer mechanisms of multiple-stage porphyry copper mineralization at Butte, Montana: vein formation by hypogene leaching and enrichment of potassium silicate protore. *Econ Geol* 74:556-589
- Bush AL, Bromfield CS (1966) Geologic map of the Dolores Peak Quadrangle, Dolores and San Miguel Counties, Colorado. *US Geol Surv, Geol Quad Map GQ-536*
- Cathelineau M (1988) Cation site occupancy in chlorites and illites as a function of temperature. *Clay Miner* 23:471-485
- Cathelineau M, Izquierdo G (1988) Temperature-composition relationships for authigenic clay minerals in the Los Azufres geothermal system. *Contrib Mineral Petrol* 100:418-428
- Cross W, Ransome FL (1905) Description of the Rico quadrangle. *US Geol Surv Geol. Atlas, Folio 130*
- Cross W, Spencer AC (1900) Geology of the Rico Mountains. *US Geol Survey 21st Ann Rept, pt 2: 7-165*
- Cunningham CG, Naeser CW, Cameron DE, Barrett LF, Wilson JC, Larson PB (1987) The Pliocene paleothermal anomaly at Rico, Colorado, as related to a major molybdenum deposit. *Geol Soc Am Abstr Prog* 19:268-269
- De Donder T, Rysseberghe PV (1936) *Affinity*. Stanford University Press, Stanford
- Helgeson HC, Delaney JM, Nesbitt HW, Bird DK (1978) Summary and critique of the thermodynamic properties of rock-forming minerals: *Am J Sci* 278-A

- Hildebrand FB (1974) Introduction to numerical analysis. McGraw-Hill, New York
- Hower J, Mowatt TC (1966) The mineralogy of illites and mixed-layer illite/montmorillonites. *Am Mineral* 51:825–854
- Larson PB (1987) Stable isotope and fluid inclusion investigations of epithermal vein and porphyry molybdenum mineralization in the Rico mining district, Colorado. *Econ Geol* 82:2141–2157
- Larson PB, Taylor HP Jr (1987) Solfataric alteration in the San Juan Mountains, Colorado: oxygen isotope variations in a boiling hydrothermal environment. *Econ Geol* 82:1019–1036
- Larson PB, Zimmerman BS (1991) Variations in  $\delta^{18}\text{O}$  values, water/rock ratios, and water flux in the Rico paleothermal anomaly, Colorado. In: Taylor HP Jr, O'Neil JR, Kaplan I (eds) *Stable isotope geochemistry: a tribute to Sam Epstein* (Geochem Soc Spec Pub 3). pp 463–469
- McDowell SD, Elders WA (1980) Authigenic layer silicate minerals in Borehole Elmore 1, Salton Sea Geothermal Field, California, USA. *Contrib Mineral Petrol* 74:293–310
- McDowell SD, Elders WA (1983) Allogenic layer silicate minerals in borehole # 1, Salton Sea Geothermal Field, California. *Am Mineral* 68:1146–1159
- McKnight ET (1974) Geology and ore deposits of the Rico district, Colorado. US Geol Surv Prof Pap 723
- Meyer C, Hemley JJ (1967) Wall rock alteration. In: Barnes HL (ed) *Geochemistry of hydrothermal ore deposits*. Holt Rinehart and Winston, New York, pp 166–235
- Naeser CW, Cunningham CG Jr, Marvin RF, Obradovich JD (1980) Pliocene intrusive rocks and mineralization near Rico, Colorado. *Econ Geol* 75:122–127
- Norton DL (1982) Fluid and heat transport phenomena typical of copper-bearing pluton environments. In: Tittley SR (ed) *Advances in geology of the porphyry copper deposits, southwestern North America*. University of Arizona Press, Tucson, pp 59–72
- Norton DL (1984) Theory of hydrothermal systems. *Ann Rev Earth Planet Sci* 12:155–177
- Norton DL, Knight JE (1977) Transport phenomena in hydrothermal systems: cooling plutons. *Am J Sci* 277:937–981
- Pratt WP (1976) Preliminary geologic map of the Hermosa Peak Quadrangle, Dolores, San Juan, La Plata, and Montezuma Counties, Colorado. US Geol Surv Open File Report 76-314
- Pratt WP, McKnight ET, DeHon RA (1969) Geologic map of the Rico Quadrangle, Dolores and Montezuma Counties, Colorado. US Geol Surv Geol Quad Map GQ-797
- Ransome FL (1901) The ore deposits of the Rico Mountains, Colorado. US Geol Surv 22nd Ann Rept, pt. 2:229–398
- Robie RA, Hemingway BS, Fisher JR (1978) Thermodynamic properties of minerals and related substances at 298.15 K and 1 bar ( $10^5$  Pascals) pressure and at higher temperatures. US Geol Surv Bull 1452
- Steven TA, Lipman PW (1976) Calderas of the San Juan Volcanic Field, southwestern Colorado. US Geol Surv Prof Pap 958
- Villas RN, Norton D (1977) Irreversible mass transfer between circulating hydrothermal fluids and the Mayflower stock. *Econ Geol* 72:1471–1504
- Wcaver CE, Pollard LD (1973) The chemistry of clay minerals. In: *Developments in Sedimentology* 15. Elsevier, Amsterdam.

Editorial responsibility: I.S.E. Carmichael